



Insights into thallium adsorption onto the soil, bamboo-derived biochar, and biochar amended soil in Pomelo orchard

Alexis Kayiranga^{1,2} · Zhuanxi Luo^{1,3} · Jean Claude Ndayishimiye^{1,2} · François Nkinahamira^{1,2} · Eric Cyubahiro^{1,2} · Theogene Habumugisha^{1,2} · Changzhou Yan¹ · Jianhua Guo¹ · Zhuo Zhen¹ · Alexandre Tuyishimire^{1,2} · Hildebrand Didier Izabayo⁴

Received: 5 January 2021 / Accepted: 18 March 2021
© Shenyang Agricultural University 2021

Abstract

Little information is available on thallium (Tl) adsorption onto biochar amended soil for a relatively long term. In this study, bamboo-derived biochar (BDB), soil in pomelo orchard (SP), and biochar amended soil in pomelo orchard (BSP) were thus used to evaluate the potential remediation of thallium (Tl) using batch-adsorption techniques. Furthermore, we characterized the above-mentioned sorbents' properties related to Tl adsorption to understand Tl's adsorption mechanisms. The results showed that BDB, SP, and BSP achieved equilibrium adsorption capacity of 96.9, 95.43, and 96.76%, respectively, within the initial 15 min. This means that compared to other sorbents, BSP exhibited an efficient sorbent for Tl remediation even when applied in the agricultural field for one year. Multi-layer adsorption played a dominant role in the adsorption of Tl, which was supported by the suitability of Freundlich model for describing the adsorption behavior of Tl onto the selected sorbents. In addition, the pseudo-second kinetic order models strongly fitted Tl's adsorption onto BDB, SP, and BSP, indicating that the process was accompanied by chemical adsorption. Observed on the surface of BDB by a Fourier Transform Infrared Spectrometer (FTIR) and an X-ray photoelectron spectroscopy (XPS), the presence of O–H groups and PO_4^{3-} might promote chemical adsorption of Tl onto BDB. Overall, these findings can provide insights into comprehensively developed bamboo-derived biochar technology to remediate Tl contamination in agricultural soils.

Keywords Bamboo-derived biochar · Pomelo orchard · Thallium adsorption · Soil remediation · Long term application

1 Highlights

Bamboo derived biochar is efficient for Tl adsorption

The dominant mechanisms of Tl adsorption were precipitation and ion exchange

The pseudo-second-order kinetics and the Freundlich model dominated the adsorption process

The adsorption of Tl onto BDB, SP and BSP reached equilibrium rapidly

2 Introduction

Various heavy metals such as cadmium (Cd), lead (Pb), arsenic (As), zinc (Zn), chromium (Cr), and thallium (Tl) have been released into the soil and environments due to a rapid population growth, development of social economy, industry activities, smelting and mining operations, waste disposal, and the extensive application of pesticides and chemical fertilizers in agriculture. These metals were reported to be highly toxic even at trace concentration (Cai et al 2019; Zhang et al. 2012), which led to serious environmental pollution and threatened human health. Particularly, the United States Environmental Protection Agency has listed Tl as a devastating contaminant that needs to be controlled (Luo et al. 2020; USEPA 2009). Specifically, 2000–5000 tons of

✉ Zhuanxi Luo
zxluo@163.com; zxluo@hqu.edu.cn

¹ Institute of Urban Environment, Chinese Academy of Sciences, Xiamen 361021, China

² University of Chinese Academy of Sciences, Beijing 100049, China

³ College of Chemical Engineering, Huaqiao University, Xiamen 361021, China

⁴ College of Agricultural, Animal Science and Veterinary Medicine (UR-CAVM), University of Rwanda, Butare, Rwanda

Tl were released into the environment through industrial and mining activities (Kazantzis 2000; Luo et al. 2020). In addition, Tl was also reported to contaminate agricultural soils through sewage sludge from wastewater treatment plants (Cai et al. 2019; D.-J. Kim et al. 2016). Consequently, the enrichment of Tl release in the agricultural soil is still increasing in many developing countries, resulting in Tl contamination and consequent adverse health effects (Li et al. 2017; Xiao et al. 2012). Therefore, it is necessary to develop proper technologies to control Tl contamination in agriculture due to its potential health risks.

Adsorption has been considered to be the most promising technology and a widely applied method that can immobilize Tl in the soil. This method is simple, low-cost, profitable, high-efficiency and environment-friendly (Sizmur et al. 2016; Zhong et al. 2016). Adsorption can remove soluble and insoluble pollutants effectively without generating hazardous by-products (He et al. 2017). However, there are still some unresolved problems associated with this application namely low adsorption rate. As a suitable adsorbent material, it possesses many special adsorptive physical–chemical properties such as: (1) the resistance to chemical/biological degradation, which makes it stay in the soil for a long time, (2) multiple numbers of functional groups available on the surface, and (3) a typical porous structure attached to some irregular granules which significantly affect the basic properties of soil like pH, electrical conductivity (EC), and alkali metals. Furthermore, biochar is an organic carbon-rich material produced by pyrolysis of organic matter, such as agricultural bio-waste, coconut fiber and bamboo biomass. Biochar has been shown to be potentially attractive to contaminated soils' deployment (Beesley et al. 2011; Ye et al. 2015; Wu et al. 2017; Safari et al. 2019; Qiao et al. 2019).

Previous studies showed that Tl adsorption onto biochar is governed by various mechanisms, such as surface precipitation, adsorption specifically via formation of surface complexes between Tl cation and organic function groups of biochar, and sorption through electrostatic interaction between Tl cation and negatively charged biochar (Li et al. 2018; Wu et al. 2017). Additionally, electrostatic adsorption capacity mostly relates to pH value, which always predominates during the adsorption process (Ye et al. 2015). The reported mechanisms augmented the immobilization of Tl in acidic soils and thus reduced its movement and bioavailability in the soils through the incorporation of biochar (Jiang et al. 2012a, b). Due to the surface heterogeneity and well-distributed pores, Tl's adsorption affinity by biochar was high (Kasozzi et al. 2010). Furthermore, the large specific surface areas and pore volumes of biochar could result in a high adsorption affinity for Tl, where Tl ions would be adsorbed on the surface of biochar or retained within their pores (Peng et al. 2017). Fang et al. (2014) exhibited that biochar had numerous function groups like $-COOH$, $C-O$,

and $-OH$, which can interact with Tl to make complexes (Dong et al. 2011). A study conducted by Shen et al. (2016) and Ahmad et al. (2014) indicated that biochar applied in the agricultural soil showed a remarkable ability to adsorb Tl metal as a single contaminant chosen from a group of heavy metals in contaminated soil, whereas decreasing the potential of Tl and other pollutants that can be up taken by agricultural soil. Thus, when well deployed in soil, biochar could reduce Tl mobility and bioavailability in soil due to its potentiality to extract thallium in soil by quickly changing the properties of soils and the chemical behavior of Tl (Jiang and Xu 2013). However, little information is available on the application of biochar in the field since current studies have been reported at lab scale. As a result, long-term biochar application in the field deserves more attention to improve our knowledge on Tl remediation in soils.

To the best of the authors' knowledge, no research has yet investigated the application of bamboo-derived biochar (BDB) in the field for one year to amend the soil with Tl contamination in Pomelo orchard. In this study, we hypothesized that BDB's adsorption capacity for Tl might be higher than that of soil in pomelo orchard (SP), and the biochar amended soil in pomelo orchard (BSP). Accordingly, the aim of this work was to characterize the above-mentioned sorbents' properties and to investigate the comparative characteristics of Tl adsorption onto BDB, SP, and BSP. Specifically, to better understand their potential mechanisms, the environmental effects of solid–liquid ratio, temperature, ion strength, and influence of solution pH on the above-mentioned sorbents for Tl adsorption process were also described in details. The results could provide insights into the effective biochar adsorbent with rapid adsorption rate and excellent adsorption capacity, which is helpful to develop suitable technologies that may show the ultimate potential for future applications in the remediation of Tl.

3 Materials and methods

3.1 Biochar preparation, characterization and tested reagents

Bamboo-derived biochar (BDB) was purchased from the Xinshiji Company in Zhejiang Province as thallium sorbents since there is abundant bamboo plantation in our studied area, Fujian Province, Southern China. The purchased BDB was produced via the pyrolysis process at a temperature ranging from 300 to 500 °C. Specifically, the BDB's pH and electrical conductivity were determined at a ratio of 1:5 (w/v) after shaking for 1 h at room temperature (Ahmad et al. 2013). The surface morphology of the BDB was detected using a scanning electron microscopy (SEM- Hitachi S – 4800, Tokyo, Japan). The functional

groups present in BDB sample were evaluated using Fourier Transform Infrared Spectroscopy (FTIR Thermo Scientific iS10), with a spectrum range of $4000\text{--}500\text{ cm}^{-1}$ at a resolution of 4 cm^{-1} . The specific surface area was examined by Brunauer–Emmett–Teller (BET) analysis (Merck-TriStar 3000, Darmstadt, Germany). The zeta potential was determined using a ZetaPALS analyzer (Malvern Instruments, Malvern, United Kingdom). In brief, 0.01 g of BDB was firstly weighed and mixed with a prepared number of aqueous solutions of 20 mL of 0.1 M of NaNO_3 solution; thus, initial pH of value 1, 3, 4, 5, 6, 7, 8, 9, 10, 11 and 12 have been adjusted using a solution of 0.1 M of HNO_3 and 0.1 M of NaOH . The containers were shaken for 24 h; after filtration and detecting the supernatant, the final pH was recorded. The intersection of pH_{final} versus $\text{pH}_{\text{initial}}$ curve and the bisector gives pH_{pzc} value (Ben-Ali et al. 2017; Peng et al. 2017; Zhong et al. 2016). The binding energy on the surface of BDB was determined by X-ray photoelectron spectroscopy (XPS; Axis Ultra DLD, Kratos, UK) using an Al $K\alpha$ line (15 kV, 10 mA, 150 W) as the radiation source (Xu et al. 2020). Then, the BDB was characterized with different parameters such as total and available contents of the alkali elements (Ca, Mg, K, and Na), the mineral particles (sand, silt, and clay) (Yolcubal et al. 2004), total organic carbon, total nitrogen contents (TOC and TN), the percentage of carbon, nitrogen, sulfur and their molar element ratios of O/C and (N + S + C)/C. Additionally, national standard Tl sample solution (1000 mg L^{-1}) was also purchased from China's National Center of Analysis. Concentrated nitric acid (GR, guarantee reagent) and hydrofluoric acid (GR, guarantee reagent) were produced by Sino Pharm Chemical Reagent Co., Ltd., China. All the chemical solutions were prepared using distilled water ($18\text{ M}\Omega\text{ cm}$, Milli-Q water).

3.2 Soil sampling and characterization

The purchased BDB was applied into the soil with 5% to amend soil Tl contamination using several tested pots in the field of pomelo orchard. After one year, we collected the samples from the above-mentioned pots to get the homogeneously mixed sorbents (BSP). Simultaneously, SP was collected randomly at the depth of 0–20 cm to compare its adsorption of thallium with that of the BDB. After hand-picked removal visible plant debris, roots, and the gravels, the samples were placed in sterile polyvinylchloride sealed bags and transported to the laboratory within 24 h. The SP and BSP samples were naturally dried at room temperature for 2 weeks, crushed manually using ceramic mortar, then mixed symmetrically, and passed through a 2 mm nylon sieve for further test. These soil samples were analyzed for their pH as one of the most prominent factors influencing the adsorption of thallium (Xu et al. 2016), and electrical conductivity (EC). Both pH and EC were measured

electrometrically at a ratio of 1:5 (w/v) (Z. Sun et al. 2020). The SP and BSP samples were also characterized for their total organic carbon (TOC) and total nitrogen contents (TN), using an automated total organic carbon analyzer (TOC-VCPH 1000). The percentage of carbon, nitrogen, and sulfur was analyzed by CNS elemental analyzer (Vario Max, Vario MACRO, Germany elemental). The percentage of oxygen in all samples was calculated using the following equation (Abdin et al. 2020):

$$\text{O}\% = 100\% - (\text{N} + \text{S} + \text{C},\%) \quad (1)$$

Due to the elemental composition, the molar element ratios of O/C and (N + S + C)/C were also calculated seriously. Acid digestion procedures include digestion with concentrated sulfuric acid, and perchloric acid was used to investigate total phosphorus (TP) in the SP and BSP samples; its concentrations were measured using ICP-OES (Inductively Coupled Plasma Optical Emission Spectrometer, Optima 7000DV, PerkinElmer USA). Total and available contents of the alkali elements (Ca, Mg, K and Na) of the SP and BSP were determined using ICP-OES (Inductively Coupled Plasma Optical Emission Spectrometer, Optima 7000DV, PerkinElmer USA). The mineral particles in SP and BSP (sand, silt, and clay), which represent the soil texture, were measured by particle size analyzer (Marvern Mastersizer-2000) according to Yolcubal et al. (2004). The specific surface area of the SP and BSP samples was examined by Brunauer–Emmett–Teller (BET) analysis (Merck-TriStar 3000, Darmstadt, Germany). Morphology of SP and BSP was measured using a scanning electron microscope (Hitachi S-4800, Tokyo, Japan) to observe a typical porous structure attached to some irregular granules. The binding energy on the surface of SP and BSP was determined by X-ray photoelectron spectroscopy (XPS; Axis Ultra DLD, Kratos, UK) using an Al $K\alpha$ line (15 kV, 10 mA, 150 W) as the radiation source (Munirathnam et al. 2016; J. Xu et al. 2020).

3.3 Batch adsorption experiments

To investigate Tl's adsorption on the BDB, SP, and BSP, 0.25 g of each sample was mixed with 25 mL of Tl in 50 mL solution in centrifugal tubes. Herein, the Tl concentrations were composed of lower levels ranging from 5 to $100\text{ }\mu\text{g L}^{-1}$ due to its higher toxic effects. Additionally, the initial pH and temperature of this solution were set at 7 and $25\text{ }^\circ\text{C}$, respectively (Abdin et al. 2020). After being shaken (at 220 rpm) for 2 h, the tubes were centrifuged at 3000 rpm for 10 min, and Tl concentration in the supernatant was then determined using an ICP-MS (Inductively Coupled Plasma Mass Spectrometry-Agilest 7500CX). The amounts of Tl adsorbed on BDB, SP, and BSP, q_e ($\mu\text{g g}^{-1}$), were calculated using the equation below:

$$q_e = (C_i - C_e) * V/M \quad (2)$$

where q_e is the amount of Tl sorbed by BDB, SP, or BSP at equilibrium; C_i and C_e ($\mu\text{g L}^{-1}$) are the initial and equilibrium Tl concentrations of the studied solutions, respectively. M is the mass of the adsorbent (g), and V (L) is the aqueous solution volume. The efficiency of Tl removed by BDB, SP, and BSP was determined by using the following equation (Eq. 3) (Shirzadi and Nezamzadeh-Ejhi, 2017).

$$RE = \left(\frac{C_i - C_e}{C_i} \right) \times 100 \quad (3)$$

where RE designates the removal efficiency of Tl.

The adsorption levels at equilibrium were fitted to two isotherm models, as well as the Langmuir and Freundlich model (Eq. 4–5), respectively. The linear equations of adsorption isotherm models are expressed as follows:

$$q_e = \frac{q_m k_L C_e}{1 + k_L C_e} \quad (4)$$

$$q_e = k_f C_e^{1/n} \quad (5)$$

Where q_e is the adsorption level at equilibrium ($\mu\text{g g}^{-1}$); q_m designates the maximum adsorption capacity proportional to complete monolayer coverage ($\mu\text{g g}^{-1}$); C_e is the initial equilibrium concentration of Tl in solution ($\mu\text{g L}^{-1}$); k_L is the Langmuir adsorption constant ($\text{L } \mu\text{g}^{-1}$); k_f is the Freundlich adsorption constant ($\text{L } \mu\text{g}^{-1}$); n indicates how favorable the adsorption process; Linearity if convex ($n < 1$), linear ($n = 1$), or concave if ($n > 1$).

Adsorption kinetics such as the pseudo-first-order kinetic model and pseudo-second-order kinetic model were investigated to analyze the adsorption mechanisms of Tl onto sorbents. The linear equations of these selected adsorption models are expressed in the number of the Eqs. (6–7), respectively.

$$\ln(q_e - q_t) = \ln q_e - k_1 t \quad (6)$$

$$\frac{t}{q_t} = \frac{1}{k_2 q_e^2} + \frac{t}{q_e} \quad (7)$$

where q_e and q_t designate adsorption levels at equilibrium and at time t ($\mu\text{g g}^{-1}$), respectively, k_1 and k_2 are the rate constants of pseudo-first-order model (min^{-1}) and pseudo-second-order model ($\text{g } \mu\text{g}^{-1} \text{min}^{-1}$) which can be calculated from linear slope of $\log(q_e - q_t)$, vs t and t/q_t vs t plots, respectively. The influences of ionic strengths on adsorption of Tl into BDB, SP, and BSP were examined by the salt of NaNO_3 concentrations ranging from 0.01 to 0.15 mol L^{-1} within 24 h contact time (at initial pH = 7; sorbent dose was 10 g L^{-1}) (Li et al. 2017). Furthermore, we examined the

effect of pH with a range of 2 to 10 pH in the batch adsorption experiments. The effects of agitation speeds and the temperature were also examined to designate a comparative study for adsorption of Tl on BDB, SP, and BSP at a different speed and temperature of 90, 120, 150, 180, 220 rpm, 25 ± 1 °C, 35 ± 1 °C, 40 ± 1 °C and 45 ± 1 °C, respectively. The Tl concentrations in the supernatant were determined by ICP-MS (Inductively Coupled Plasma Mass Spectrometry-Agilest 7500CX) to obtain their adsorption parameters on the tested samples.

3.4 Statistical analysis

The analytical data were presented as mean values with standard errors. Statistical significance was performed using a One-Way ANOVA in SPSS 17.0. Data processing for multiple comparisons was analyzed using origin lab version 2018 (Origin lab Corporation, Northampton, MA, USA). KRATOS analytical software was used to analyze the binding energy position in the sorbents.

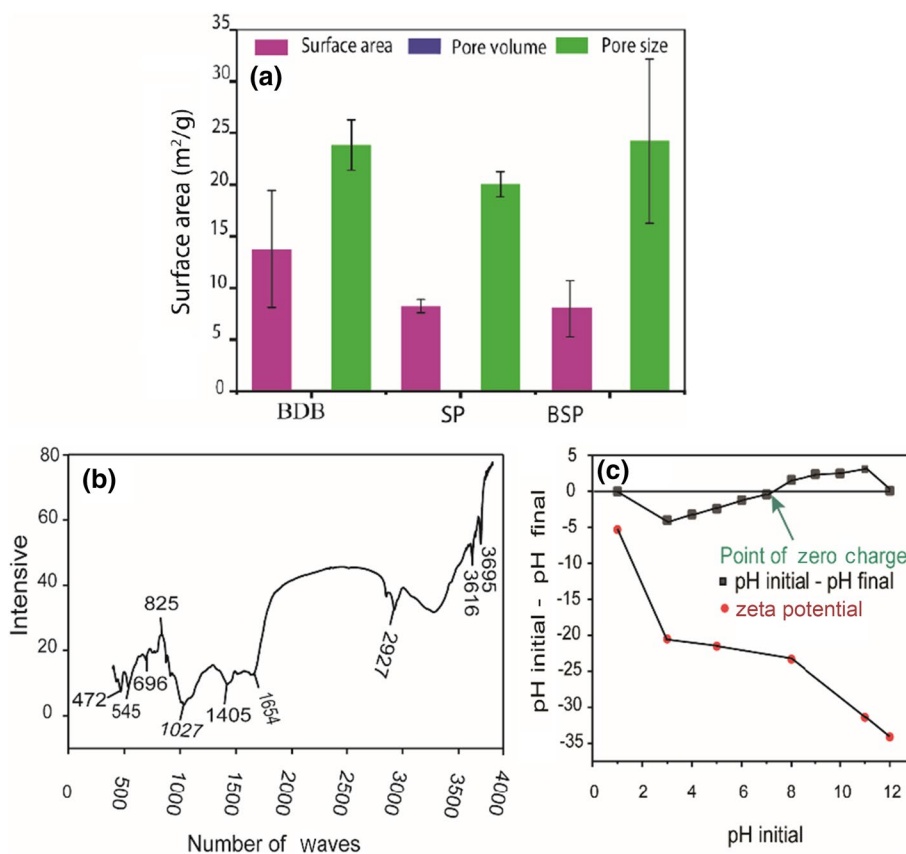
4 Results and discussion

4.1 Biochar and soil samples characterization

4.1.1 Physical and chemical characterization of Bamboo derived biochar

Biochar offers excellent characteristics as sorbent/amendment for heavy metals in contaminated soil, essentially depending on its properties such as porous structure, large surface area, and the existence of functional groups (Luo et al. 2020). In this study, BDB was observed to have the highest surface area, $13.75 \text{ m}^2 \text{ g}^{-1}$, and pore volume ($0.06 \text{ cm}^3 \text{ g}^{-1}$), comparable with the values of SP and BSP with 8.24, and $7.97 \text{ m}^2 \text{ g}^{-1}$, respectively. Consistently, the BDB possessed average adsorption pore width, average adsorption pore diameter, and desorption average pore diameter since their total average pore size was 23.87 nm (Fig. 1a). Although a little lower pore size was observed for BDB (23.87 nm) than that of BSP (24.23 nm), it is observed to possess a higher pore size when compared with that of SP as shown in (Table S1). A study conducted by Xiang et al. (2020) witnessed that BDB with a higher specific surface area could be associated with its porous structure. Additionally, BDB used in our study revealed different functional groups that were vigorous to increase the adsorption of thallium through its surface area (Fig. 1b). As shown in Table S2, there were various characteristics of adsorption of bands found in the FTIR spectra of BDB: the band at 3616 and 3695 cm^{-1} confirmed the presence of a strong alcohol (O–H alcohol-stretching), which can promote Tl adsorption

Fig. 1 Physical–chemical properties of the BDB, SP and BSP: (a) The BET surface area, cumulative volume of pores and pore size, (b) Results of the FTIR spectra analysis of bamboo-derived biochar pyrolyzed at 300–500 °C, (c) Extractive curves of point of zeta charges and zeta potential



performance via complexation mechanism (Huosheng Li et al. 2018; Tang et al. 2019). The peak at 2927 cm⁻¹ showed the presence of strong hydrocarbons compounds (C-H alkanes- stretching), and band at 1654 cm⁻¹ was assigned to C=C variable alkene-stretching; there were bands at 1405 and 825 cm⁻¹ which were assigned to aromatic compounds (C-C alkanes-stretching, and C-H), respectively. The bands at 472 and 696 cm⁻¹ corresponded to C-H bending alkynes. The peak appeared at 545 cm⁻¹, exhibiting the presence of C-Br stretching (Alkyl halides). Moreover, a peak observed at 1027 cm⁻¹ could represent the availability of C-O stretching carbonyl.

Furthermore, the zeta potential is a prominent parameter for the stability of colloidal dispersion. The positive and negative signs and the zeta potential's magnitude exhibit the degree of electrostatic attraction or repulsion between charged particles in a dispersion (H. Zhang et al., 2020a, b). The zeta potential of BDB varied from -5.3 to -34.1. Their values were negative charges, which decreased with increasing pH, as indicated in Table S2. As shown in Fig. 1c, the intersection pH_{final} versus pH_{initial} curves and the bisector gives a point of zero charges (pH_{pzc} value). The pH_{pzc} value was found to be 7, where the effect of pH could also be explained by considering the point of zero charges of the adsorbent (pHpzc). Therefore, the adsorbent's surface charge was negatively charged at pH ≥ 7, and it became positively

charged at pH < 7. At pH ≥ 7, the adsorption would be favorable because of electrostatic attraction between metal ions and adsorbents. The deprotonation of acidic functional groups of the surface of BDB would be the cause of zeta potential curves towards negative values (Jiang et al. 2012a, b).

4.1.2 Characterization of soil in Pomelo and Biochar amended soils

Selected parameters of SP, BSP, and BDB are presented in Table S3. The particle present in SP and BSP is classified as a sand particle with the known value of particle size of 0.0625 and 0.0609 mm, respectively (Yolcubal et al. 2004). However, this amount of sizes showed that there is no significant difference at 5% level of significance ($P = 0.474 > 0.05$). In contrast, we found a significant difference at 5% level of importance on BDB with other soil samples ($P < 0.05$). SP and BSP were slightly acidic and not significant at 5% level ($P > 0.05$), and electrical conductivity (EC) values were 141.7 μs cm⁻¹ and 110.33 μs cm⁻¹ (Fig. S1), respectively. BDB was very alkaline with high pH and EC of 8.03 and 2560 μs cm⁻¹, respectively, suggesting that higher pyrolysis temperature led to higher pH of the BDB (Yuan et al. 2011). The increased amount of EC in BDB may be due to the high contents of Na, K, Ca, and Mg in BDB (Fig. S1) (Jamari et al. 2016).

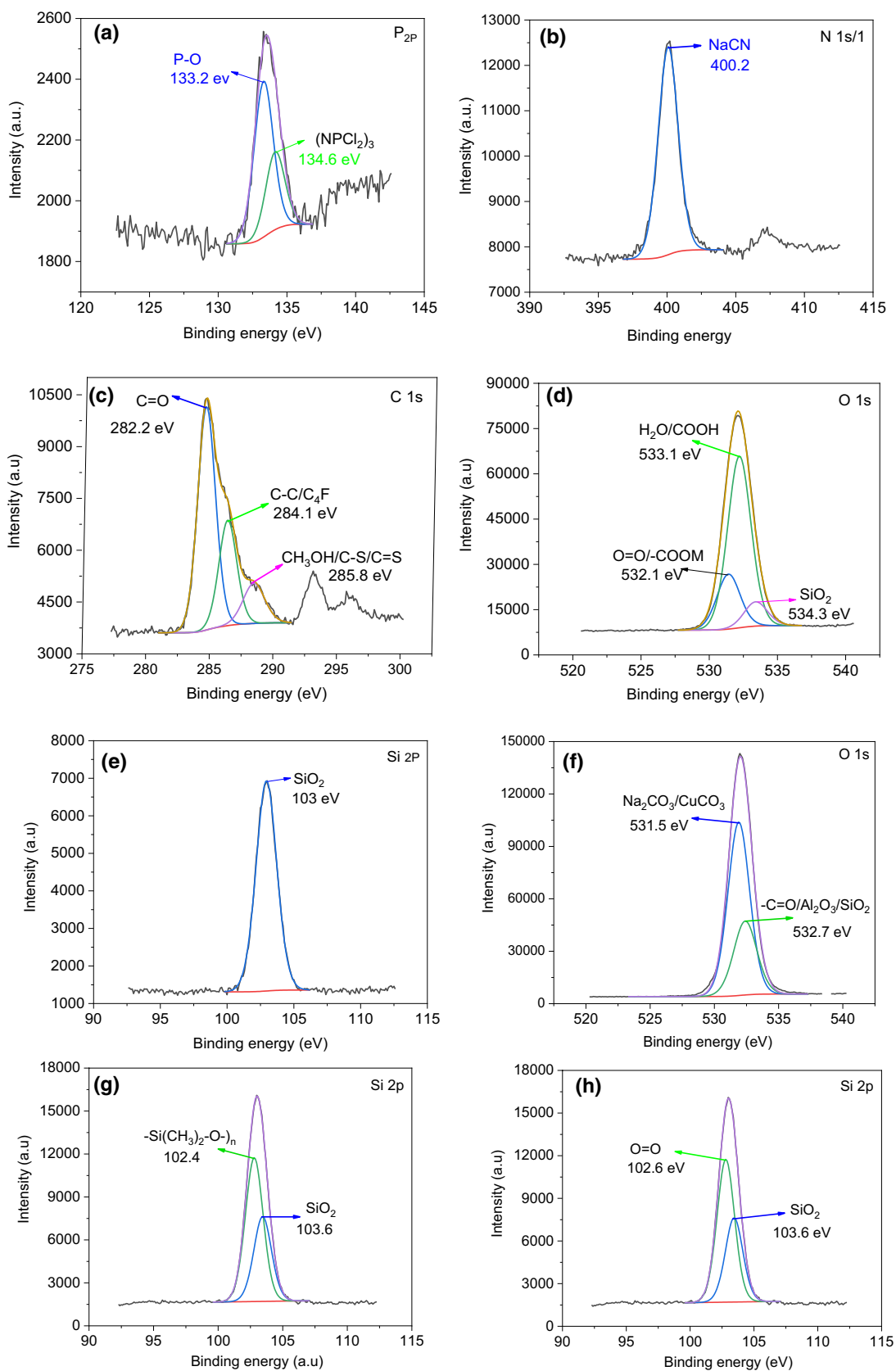


Fig. 2 XPS analysis of the spectra P 2p, N 1 s, C 1 s, O 1 s, and Si 2p: (a–e) indicate the binding energy and corresponding bonds on BDB, (c) exhibits the similar bonds and binding energy to BDB, SP and BSP, (f) similar bonds and binding energy to SP and BSP, and 2(g–h) exhibit the binding energy and corresponding bonds on SP and BSP, respectively

Furthermore, the amounts of the total and available contents of the alkali elements (Na, Mg, K, and Ca) were low in BSP than those in SP (Fig. S1). The relative proportion of these above-mentioned elements, as well as their total amount in the SP and BSP depends mainly on the soil parent material, whereby they may coexist in soil and compete for the active sites on the adsorbents with TI; thus, their negative effect becomes more obvious with increasing their concentrations (Tang et al. 2019). Additionally, the differences in alkali elements (Na, Mg, K, and Ca) between SP and BSP were not significant ($P=0.46, 0.390, 0.887, \text{ and } 0.327$, respectively).

Additionally, the elemental compositions of BDB, SP, and BSP were reported to be a useful indicator for understanding their nature and adsorption affinity. As a major component of BDB, the carbon percentage was much higher than that in the SP and BSP (Table S1). The increases in carbonization degree were caused by increasing aromatic compounds during BDB production using pyrolysis methods at high temperatures in oxygen-limited conditions (Abdin et al. 2020). As shown in Table S3, the amount of total organic carbon (TOC) in BDB was higher due to the relatively high amount of organic and inorganic carbon present in bamboo woods, used as raw material (Gao et al. 2020; Luo et al. 2020). The percentage of oxygen in BDB was lower than that in other sorbents because it was produced in higher temperatures with limited or no oxygen (Luo et al. 2020). As a result of this, volatile compounds and OH dehydration were lost, as well as, the breakdown of aliphatic compounds that were substituted by aromatic compounds (Abdin et al. 2020; Luo et al. 2020). Furthermore, the contents of total nitrogen (TN) were higher in SP and BSP (Table S3) due to available organic and inorganic compounds containing nitrogen that were present in agricultural soils. Additionally, the percentage of nitrogen (N) in SP and BSP was lower than that in the BDB. This was probably caused by increasing N-related aromatic compounds during BDB production. Consistently, recent studies reported that BDB has high total nitrogen than SP, with amounts of 5.9 and 1.06 mg kg⁻¹, respectively (Jin et al. 2020).

Moreover, as explained by Abdin et al. (2020), pyrolysis temperature possessed a significant effect on molar element ratios of O/C and (O + N + S)/C (Table S1). The smaller amount of O/C in BDB was generally caused by dehydration, which lowers the hydrophilicity on its surfaces (Zhao et al. 2017). The lower percentage of molar (O + N + S)/C

for BDB proposed the presence of aromaticity and reduction in polarity (Abdin et al. 2020). In our present study, the O/C ratio in SP and BSP was much higher than that of BDB with 79.30, 69.92, and 4.08%, respectively. In addition, total phosphorus in BSP was significantly higher than that in SP, with concentrations of 5566.66 and 3524.54 mg kg⁻¹, respectively. This means that the application of alkaline biochar to soil significantly increased the sorption of P and decreased the availability of sorbed P.

4.1.3 Morphology of bamboo-derived biochar, soil in pomelo and biochar amended soil

Biochar demonstrated a coarse surface attached to some irregular granules and size particles with rough surfaces indicative of the porous structure (Fig. S2 a). Thus, SEM designated that BDB contained a large and typical porous structure with an oval-shaped formation, mostly owing to organic materials volatilization during the pyrolysis process. It also seems to have a lot of carbon (as described in Sect. 3.1.1), which is the reason why TI could be quickly attached to its surface. However, at high resolution, BDB exhibited loose and porous structure. By contrast, the morphology of SP was more regular, smooth, with limited porous structure and a compacted surface area (Fig. S2 b). This structure is likely to limit the adsorption of TI to its surface. By observing the SEM-delivered image, BSP exhibited less porous structure on its surface probably because it was covered by an agglomeration of small spherical particles of the soil (Fig. S2 c).

4.1.4 XPS analysis

The XPS is routinely used to evaluate the chemical states present on the surface of the samples. The XPS peaks of Ti 4f, Mn 3s, Mn 2p, Fe 2p, S 2p, C1s, O 1s, P 2p, N 1s, and Si 2p were investigated on BDB, SP, and BSP (Table S4). No Ti 4f, Mn 3s, Mn 2p, Fe 2p, S 2p signals were observed in XPS lines for all samples due to the low content of Ti, Mn, Fe, and S elements. The P 2p spectrum peaks at 132.2 eV and 134.6 eV were only found in BDB (Fig. 2a). These peaks indicated that P had been bonded to O, N, and Cl₂ atoms, which formed P-O type group and (NPCl₂)₃, containing 66.67 and 33.33% (1.63 FWHM, Full width high maximum), respectively, after the P saturate (H. Zhang et al. 2020a, b). It has been reported that TI can complex with PO₄³⁻, making a more complexation and precipitation on active surface sites (Abdin et al. 2020). The same conclusion might be drawn from the spectra of N 1 s at 400.2 eV, which bonded with Na and C atoms and formed a chemical state of NaCN (Fig. 2b). Additionally, the XPS peaks of C 1 s (282.2, 284.1 and 285.8 eV); O 1 s (532.1, 533.1, and 534.3 eV); and Si 2p (103 eV) for BDB were originated from C=C (S. J. Kim

et al. 2018), C–C/C₄F, and CH₃OH/C–S/C=S (Omachi et al. 2020) containing an atomic concentration of 63.19, 23.92, and 12.89%; O 1 s could be assigned to oxygen atoms of the carboxylic groups together with metal ion O=O/-COOM or hydrogen groups H₂O/COOH, and the presence of mineral SiO₂ with 21.9, 68.41 and 9.69% (Tselesh 2008), while the peaks Si 2p also exhibited one single SiO₂ (Fig. 2c–e), respectively. Given that these presences of oxygen atoms of the carboxylic groups and hydrogen have more contributions to Tl adsorption into BDB, the adsorption behaviours were controlled by numerous mechanisms, such as oxygen and carbon bonding interactions, ion exchange and electrostatic interaction (Haojing Zhang et al. 2020a, b).

The C 1 s peaks in SP and BSP were fitted the same component with pure BDB but differed in their atomic concentrations and FWHM (Fig. 2c, Table S4). For the O 1 s peaks (Fig. 2f), two components were fitted at 531.5 and 532.7 eV, attributed to Na₂CO₃/CuCO₃ and Al₂O₃/SiO₂ (Duan et al. 2011; Huang et al. 2017), respectively. The Si 2p in the SP and BSP indicated a similar peak centered at 103.6 eV, which was assigned to a mineral SiO₂ (Fig. 2g), but the only difference observed in the presence of the peaks -Si (CH₃)₂-O- centered at 102.4 eV, and O=O centered at 102.6 eV (Fig. 2h), respectively. The fitted elemental percentage and FWHM in each chemical state observed in all samples are shown in Table S4. The results for the Si 2p spectrum in both samples highlighted the significant role of the minerals mentioned for thallium cycling in SP and BSP, implied that SP and BSP strongly bound Tl on their surface (Wick et al. 2020).

4.2 Tl adsorption onto bamboo-derived biochar, pomelo soil and biochar amended soil

4.2.1 Effect of pH on Tl adsorption

The solution pH is a critical factor for the adsorption process in the aqueous phase because it determines the surface charge of the adsorbate-adsorbent (Ndagijimana et al. 2019). The solution pH contained a significant effect on the removal rate of Tl (Fig. 3). Pointedly, at a pH of 2, the removal rates of Tl by BDB and SP were less than 80%. Particularly, at pH 2 and 3, the removal rates for BSP were also less than 80%. This implies that the more solution pH augments, the more removal rates by BDB, SP, and BSP. Indeed, the adsorption mechanism was not usually presented under acidic conditions due to the availability of multiple numbers of functional groups on the surface of BDB, which is generally connected with excess of H⁺. That could form competitive adsorption sites with Tl (Gao et al. 2020; Y. Sun et al. 2016). Additionally, at lower pH, the carbon surface transmits positive charges, which resulted in electrostatic repulsion force with Tl particles (Sun et al. 2016). As a result, the adsorption

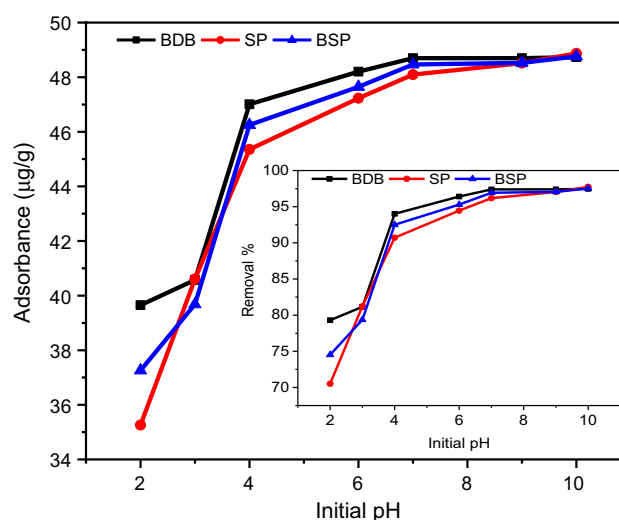


Fig. 3 Effect of pH on adsorption (the initial Tl concentration is 500 µg L⁻¹; adsorbent dose = 10 g L⁻¹; contact temperature = 25 °C; contact time = 24 h)

capacity and efficiency removal amount of Tl by BDB was partially higher compared to SP and BSP. The optimum pH range for thallium adsorption was found in the range of 7 to 9. The more pH increased from 2 to 10, the more the surface functional groups were deprotonated, which gives more chance to bind to Tl.

4.2.2 The effect of contact time and adsorption kinetics

BDB, SP, and BSP presented the highest adsorption capacity of 48.68, 47.72, and 48.38% µg g⁻¹, respectively, and their corresponding removal rates reached 97.35, 95.43, and 96.76%, respectively (Fig. 4). As a function of time, the adsorption capacity for BDB increased faster at an initial time of 2 to 15 min; thereafter, there was no significant increase up to 60 min, due to two main reasons: (1) the saturation sites on the surface of BDB, (2) the reduction of Tl concentrations in the solution as the effect of continuous adsorption with time. While in SP and BSP, the adsorption capacity was also increased faster from 2 to 15 min. Thereafter, it decreased slowly until the last time of oscillation, which was probably because most spaces on the surface area of adsorbents were fully occupied.

Moreover, various models were used to investigate the adsorption kinetics of Tl to fit the experimental data. The linear plots of adsorption kinetics models for Tl on BDB, SP, and BSP are shown in Fig. 5. And their appropriate kinetic parameters are recorded in Table S5. The lower *R*² values of the pseudo-first-order kinetic model of Tl on BDB, SP, and BSP confirmed that this model does not fit the adsorption of Tl, which indicates the lousy quality of linearization (Fig. S3). This was because the calculated values of *R*²

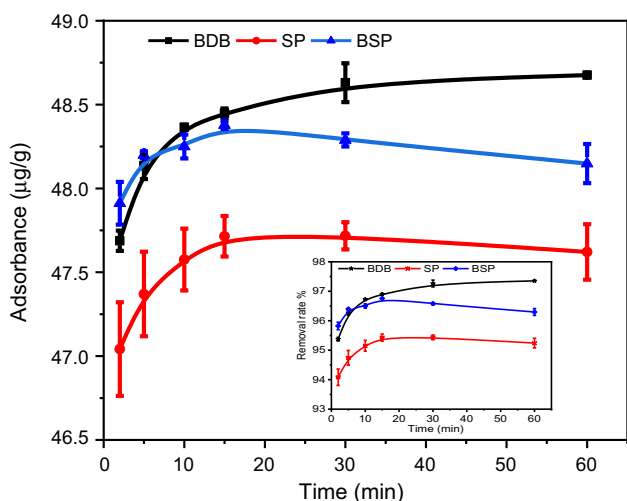


Fig. 4 Effect of contact time on adsorption (the initial TI concentration = 500 µg L⁻¹; adsorbent dose = 10 g L⁻¹; pH = 7; contact temperature = 25 °C)

were not close to 0.999 as a standard correlation coefficient. However, the correlation coefficient of the pseudo-second-order kinetic model of TI for all adsorbents was significantly higher (R^2 is near to 1), which contained good agreements with the theoretical value Q_e (Huosheng Li et al. 2018) compared to those of the pseudo-first-order model (Table S5). These correlations exhibited that the pseudo-second-order model was more suitable to predict the kinetic behavior of adsorption of TI. Similar to the previous studies reported by (Gao et al. 2020; Y. Sun et al. 2016; Zhu et al. 2016), they implied that the adsorption on all mentioned adsorbents takes place along chemical interactions dominated by ionic exchange.

4.2.3 The effect of initial concentration and solid-liquid ratio on TI adsorption

The effect of different initial concentrations on the adsorption of TI onto BDB, SP, and BSP is indicated in Fig. S4. Initially, the experimental results exhibited that, when the initial concentrations of TI increased from 5 to 20 µg L⁻¹, there was rapidly increasing in the removal rate of TI. Thereafter, the increasing moderately tended towards equilibrium at TI concentrations in the range of 50–100 µg L⁻¹. This is because the potential adsorption sites of BDB were unlimited. In SP, initially, there was a slow increase in the removal rate at TI concentrations ranging from 5 to 20 µg L⁻¹ with their appropriate adsorption capacity of 0.5 and 2 µg L⁻¹, respectively. However, when the initial concentrations were increased from 20 to 50 µg L⁻¹, no significant change was observed in the TI removal rate, due to rapidly being occupied on its surface as the initial TI concentration increased, afterwards when the initial concentration increased from 50

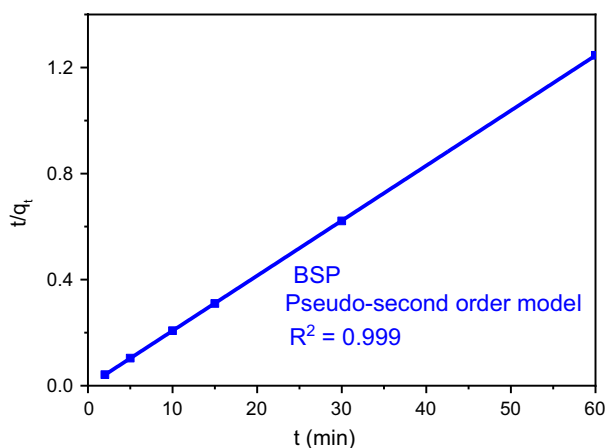
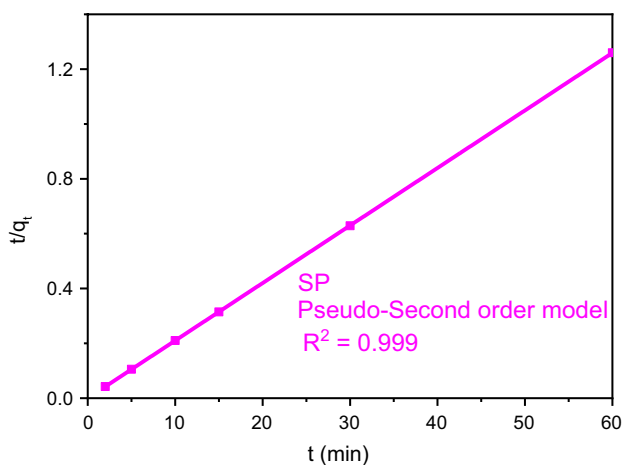
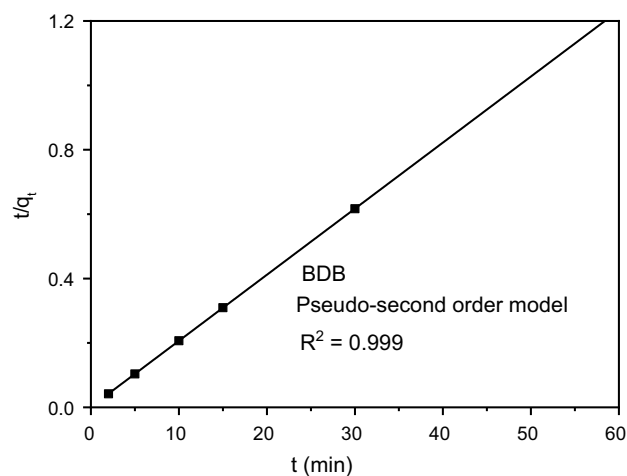


Fig. 5 The linearized form of pseudo-second-order models showing the variation of adsorption t/q_t^{-1} in the function of the variations of time for adsorption of thallium

to 100 µg L⁻¹, there was a slight decrease in the removal rate from 99.72, 99.68 and 99.63%, respectively. Except in BSP, when the initial TI concentration increased from 5 to 20 µg L⁻¹, the percentage of removal rate decreased moderately before decreasing slowly. It decreased from 99.9 and

99.8%, then became decreased slowly from 99.80, 99.79, 99.77, and 99.75% when TI concentrations were in the range of 20–100 $\mu\text{g L}^{-1}$, respectively. It is because that the adsorption sites in SP and BSP were limited and tended to be unsaturated. Nevertheless, with the increase of concentrations of TI from 5 to 100 $\mu\text{g L}^{-1}$, the adsorption capacities of TI increased sharply with overlapping linear lines for both adsorbents (Fig. S3) due to the stronger mass power transfer given by the increasing concentration of TI (Aydin et al. 2008; Gao et al. 2020).

Furthermore, the Langmuir and Freundlich isotherms equations were extensively used to explain all adsorbents' sorption equilibrium data. The former model has generally applied to assess ideal sorption concerning homogeneous sorbents (Langmuir 1918), while the later model is frequently used for non-ideal sorption controlled by complex sorption process; thus, it is considered as the best model discussing the adsorption isotherms of metal ions (Peng et al. 2017; Xiang et al. 2020). The Freundlich and Langmuir's isotherm parameters equations are summarized in Table S6. Both equations are commonly described as preferable to the isotherm data for all adsorbents. Based on the R^2 values, it is confirmed that the Freundlich isotherm could better stimulate the TI adsorption process than the Langmuir isotherm model, exhibiting that the process was not predominantly a single-molecule adsorption process. The adjusted coefficient of determination (r^2_{adjust}) ranged from 0.98–0.99 for all samples, confirming that the Freundlich model (FM) is the best choice for adsorption isotherms. The Freundlich isotherm model is shown in Fig. 6, while the Langmuir isotherm model is illustrated in Fig. S5.

Additionally, the solid–liquid ratio could be a prominent factor affecting adsorption and have many contributions to the adsorption capacity of adsorbents (Aydin et al. 2008; Gao et al. 2020). The more the solid–liquid ratio is increased, the more adsorption surface area and surface sites upon which TI can quickly attach were provided for adsorbents (Gao et al. 2020). The maximum removal rates of BDB, SP, and BSP reached 91.62, 83.18, and 88.80%, respectively (Fig. S6). With the increase of solid–liquid ratio, the efficient removal of TI on BDB, SP, and BSP increased rapidly (Fig. S5). Except for BDB at the higher solid–liquid ratio of 20 $\mu\text{g L}^{-1}$, the removal rate became equilibrium. This was possibly due to the wide distribution of micro or mesopores and the interactions (aggregation) among BDB particles at a higher solid–liquid ratio. Their surface area could decrease adsorption capacity; thus, the space of TI spreading to BDB could also be increased (Gao et al. 2020).

4.2.4 Effects of ionic strength

The ionic strength influences the thickness of the electrical double layer (Guo et al. 2019). An increase in ionic strength

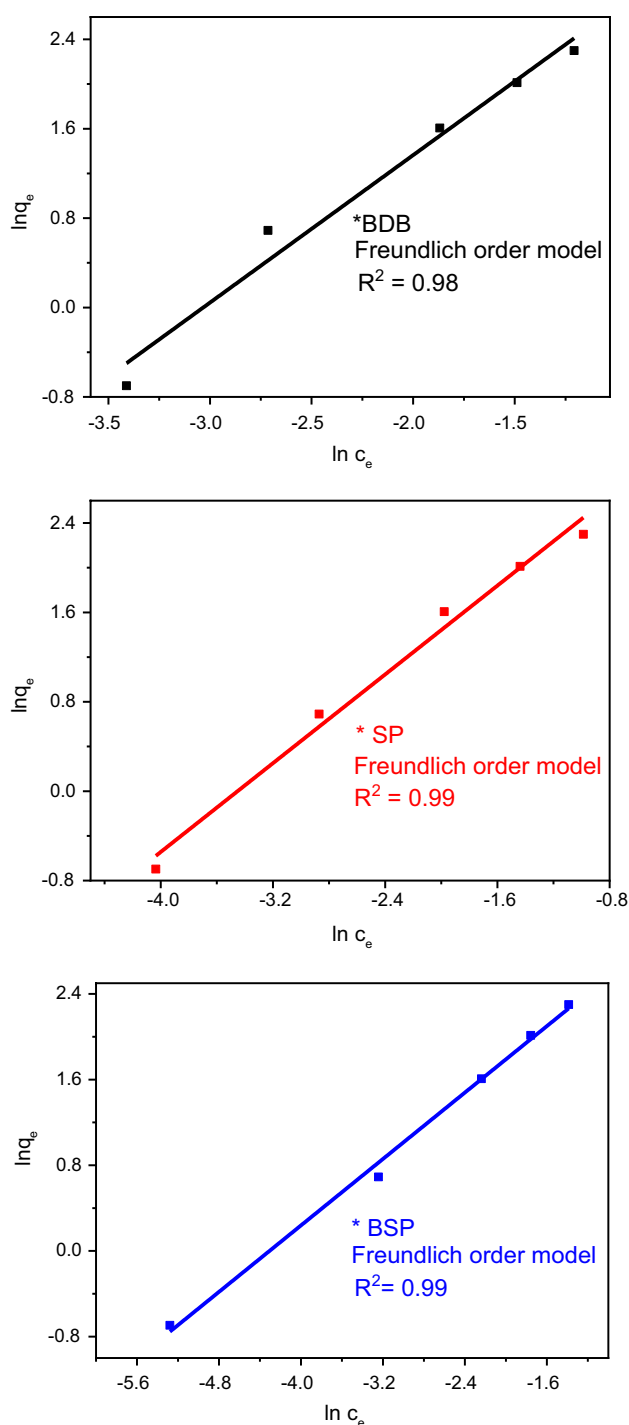


Fig. 6 Freundlich isotherm indicating the variation of $\ln q_e$ with respect to $\ln c_e$ for adsorption of TI into BDB, SP, and BSP

caused a decrease in TI adsorption and removal efficiency into BDB, SP, and BSP (Fig. S7). The decrease in TI adsorption capacity and removal rate was caused by the competition of binding sites between Na^+ and TI^+ on the surface area of adsorbents at low ionic strengths (Li et al. 2017). Unfortunately, there was an inconspicuous decrease when the ionic

strength was from 0.1 to 0.15 $\mu\text{g L}^{-1}$ but became obvious when the ionic strength ranged from 0.01 to 0.1 mol L^{-1} . This explains that at a high ionic strength of 0.15 mol L^{-1} , Na^+ did not affect a considerable decrease in Tl removal due to the electrostatic interactions, which were more sensitive to variation in ionic strength (Lalmunsiama et al., 2013).

4.2.5 Effects of agitation speed and temperature on adsorption

In this study, the range of agitation speed varied from 90 to 220 rpm while keeping the optimum dose of BDB, SP and BSP, and the optimum pH at constant. As shown in Fig. S8, the Tl removal rate of BDB commonly increased slowly with increasing agitation speed from 90–150 rpm. While in BSP, the equilibrium began at the optimum agitation speed of 180 rpm. Except in SP, Tl adsorption decreased when it reached the last oscillation speed; thus, the maximum removal rate for all adsorbents reached 180 rpm. With the increase of agitation speed, the Tl removal efficiency of BDB, SP, and BSP increased from 97.59 to 99.97%, 85.98 to 92.97%, and 86.18–98.10%, respectively, and the Tl removal efficiency of the adsorbents for a higher agitation speed remained at equilibrium. This can be explained by the fact that a higher agitation speed increases the degree of physicochemical interaction between the negatively charged surface of the adsorbents used in this study and Tl ions at acidic conditions, resulting in a higher Tl removal efficiency (Muhammad 2011). The agitation speed of 180 rpm, providing the highest Tl removal efficiency, was not selected as the highest speed for all experimental studies and used for the remaining adsorption studies. An optimum agitation speed is fundamentally recommended to maximize the interactions between metal ions and adsorption sites of all adsorbent solutions.

For the effect of temperature, the adsorption of Tl onto BDB, SP, and BSP was also examined by setting different temperatures such as 25 ± 1 °C, 35 ± 1 °C, 40 ± 1 °C, and 45 ± 1 °C. The observation indicated that the amount of adsorbed Tl on BDB, SP, and BSP favored as temperature increased; thus, the endothermic reaction is proven. With the increase of temperatures, the adsorption of Tl ions into adsorbents decreased sharply from three consecutive temperatures but became equilibrium when reached a higher temperature (Fig. S9). This is possibly due to the intraparticle diffusion decreases at a higher temperature, and more adsorption sites were not created, which limited to boost up adsorption phenomena (Batool et al. 2018).

4.3 Potential adsorption mechanism and implications

Tl mobilization in soil is demonstrated to be related to several simultaneous processes such as oxidation, reduction and

adsorption–desorption (Antic-Mladenovic et al. 2017; Rinkelebe et al. 2020). For Tl adsorption, a few components such as ionic exchange, electrostatic attraction, surface precipitation and surface complexation with functional groups are considered to be a great function (Li et al. 2018; Wu et al. 2017). In this study, as shown by FTIR and XPS results, the presence of O–H can promote chemical adsorption of Tl; This was confirmed by kinetics study which fitted well with pseudo-second order, implying chemical adsorption. Based on experimental data and results from XPS, the presence of PO_4^{3-} observed on the surface of BDB would play a certain role in the Tl uptake via complexation mechanism. Whereby, the attraction of Tl towards the active sites could be significantly affected by the protonation or deprotonation of hydroxyl groups (Fig. 7). In the chemisorption process, Tl can form complexes with oxygen (Huosheng Li et al. 2018; Tang et al. 2019). In particular, the availability of carbonyl, oxygen, carbon bonding interactions, and phenolic enables the ability to form a complex with Tl ions. These ions are primarily retained by simple ions exchange with COOH groups (Zhang et al. 2013). Furthermore, electrostatic interactions between the negatively charged groups in the adsorbents and the adsorbed Tl ions are very likely to occur based on our findings here that the adsorption capacity was increased with increasing pH (Tran et al. 2016). Additionally, supported by the suitability of Freundlich model for describing the adsorption behavior of Tl, multi-layer adsorption might play a dominant role in the adsorption of Tl.

Meanwhile, the soil is a mixture of organic and inorganic solid materials. Therefore, countless amount of organic

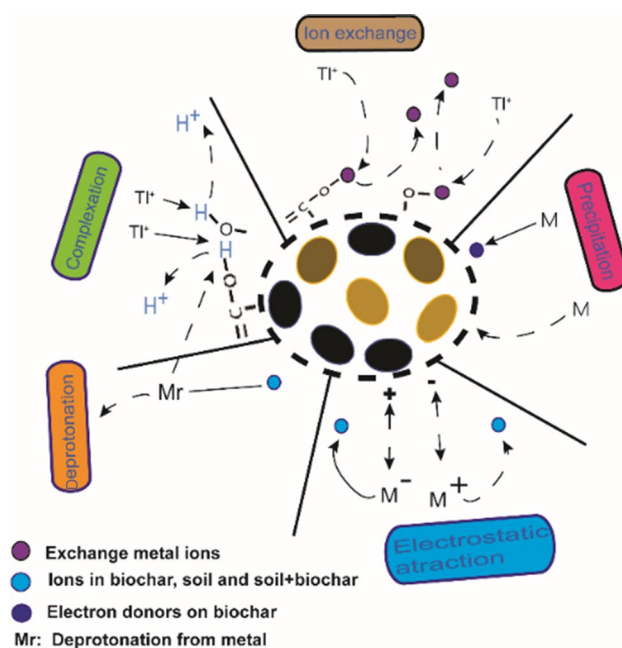


Fig. 7 Mechanism of Tl by BDB, SP, and BSP

and inorganic solutes in soil-solution systems compete for adsorption sites on solid (Covelo et al. 2004). As illustrated above, SP and BSP have also been used as adsorbents for Tl removal in aqueous solutions. Tl into SP, and BSP could be sorbed to various solid phases, which is limited in its mobility and availability because it is mostly complicated forms (Kim et al. 2016). Tl mobility and adsorption in SP and BSP-solution systems could be affected by different soil properties, including soil texture, soil reaction (pH), clay content, types and electrical conductivity (EC), which are considered as the most prominent factors influencing the adsorption of thallium (Xu et al. 2016). Accordingly, Tl mobility and availability in soil-solution systems can be determined by equilibrium isotherms and kinetic studies in target Tl adsorption mechanisms. These studies are prominent to assess the Tl adsorption capacity of BDB compared to SP and BSP. However, there is still insufficient information on the full mechanisms of Tl adsorption into SP and BSP to which warrants more attention.

From the above-mentioned adsorption data, we found that the bamboo-derived biochar can be utilized to improve soil properties to increase Tl adsorption, even for one-year application in the field scale. For the comprehensive benefits of biochar, including carbon dioxide sequestration and soil properties amendment, biochar can be substantially used in agricultural practices. However, the efficiency of biochar application and its corresponding duration are impacted by many environmental factors. Thus, it is needed to have more investigations on their duration at longer-term while biochar applied in the field.

5 Conclusion

This study mainly discussed the efficient sorption and remediation of thallium of BDB applied in the field for 1 year (BSP) while compared to SP and BDB. Considering the comparable equilibrium adsorption capacity of Tl and the comparable amount of specific surface area observed in BSP, we concluded that BDB is the suitable candidate for the adsorption of Tl from agricultural soils even when applied in the field for one year. The pseudo-second-order kinetics and the Freundlich model dominated the adsorption process to delineate Tl onto BDB, SP, and BSP, suggesting that available adsorption sites determined the adsorption capacity of Tl on them. Among the reported sorbents, BDB was also effective in removing Tl from aqueous solutions and immobilizing co-existing of Tl in the contaminated agriculture soil. The adsorption process of BDB, SP, and BSP was influenced by pH. Experimental and modelling results indicated that multiple mechanisms control Tl sorption onto BDB, SP, and BSP. Chemical interactions showed the dominance of ionic exchange mechanism, surface complexes, and surface

precipitation between Tl ions and the surface of adsorbents. Even though we mostly highlighted the adsorption mechanism by BDB, SP, and BSP, there are still uncertainties in understanding their full mechanism on Tl adsorption in agricultural soil. Additionally, it is still needed to have more investigation on BDB's longer-term duration while applied in the field. Our findings from this work exhibited that BDB is recommended to be applied to agricultural soils to immobilize Tl distribution due to its removal ability and great potential as an alternative adsorbent for environmental remediation.

Supplementary Information The online version contains supplementary material available at <https://doi.org/10.1007/s42773-021-00095-1>.

Acknowledgements This work was financially supported by the STS project of the Chinese Academy of Sciences in Fujian province (2018T3016), the Nature Science Foundation of Fujian Province (2017Y0081 and 2018J01473), and the Scientific Research Funds of Huaqiao University (605-50Y19047).

References

- Abdin Y, Usman A, Ok YS, Tsang YF, Al-Wabel M (2020) Competitive sorption and availability of coexisting heavy metals in mining-contaminated soil: contrasting effects of mesquite and fishbone biochars. *Environ Res* 181:108846. <https://doi.org/10.1016/j.envres.2019.108846>
- Ahmad M, Lee SS, Rajapaksha AU, Vithanage M, Zhang M, Cho JS, Ok YS (2013) Trichloroethylene adsorption by pine needle biochars produced at various pyrolysis temperatures. *Bioresour Technol* 143:615–622. <https://doi.org/10.1016/j.biortech.2013.06.033>
- Ahmad M, Rajapaksha AU, Lim JE, Zhang M, Bolan N, Mohan D, Ok YS (2014) Biochar as a sorbent for contaminant management in soil and water: a review. *Chemosphere* 99:19–33. <https://doi.org/10.1016/j.chemosphere.2013.10.071>
- Antic-Mladenovic S, Frohne T, Kresovic M, Stark HJ, Savic D, Licina V, Rinklebe J (2017) Redox-controlled release dynamics of thallium in periodically flooded arable soil. *Chemosphere* 178:268–276. <https://doi.org/10.1016/j.chemosphere.2017.03.060>
- Aydin H, Bulut Y, Yerlikaya C (2008) Removal of copper (II) from aqueous solution by adsorption onto low-cost adsorbents. *J Environ Manage* 87(1):37–45. <https://doi.org/10.1016/j.jenvman.2007.01.005>
- Batool F, Akbar J, Iqbal S, Noreen S, Bukhari SNA (2018) Study of isothermal, Kinetic, and thermodynamic parameters for adsorption of cadmium: an overview of linear and nonlinear approach and error analysis. *Bioinorg Chem Appl* 2018:3463724. <https://doi.org/10.1155/2018/3463724>
- Beesley L, Moreno-Jimenez E, Gomez-Eyles JL, Harris E, Robinson B, Sizmur T (2011) A review of biochars' potential role in the remediation, revegetation and restoration of contaminated soils. *Environ Pollut* 159(12):3269–3282. <https://doi.org/10.1016/j.envpol.2011.07.023>
- Ben-Ali S, Jaouali I, Souissi-Najar S, Ouederni A (2017) Characterization and adsorption capacity of raw pomegranate peel biosorbent for copper removal. *J Clean Prod* 142:3809–3821. <https://doi.org/10.1016/j.jclepro.2016.10.081>
- Cai LM, Wang QS, Wen HH, Luo J, Wang S (2019) Heavy metals in agricultural soils from a typical township in Guangdong Province,

- China: occurrences and spatial distribution. *Ecotoxicol Environ Saf* 168:184–191. <https://doi.org/10.1016/j.ecoenv.2018.10.092>
- Chen B, Chen Z, Lv S (2011) A novel magnetic biochar efficiently sorbs organic pollutants and phosphate. *Bioresour Technol* 102(2):716–723. <https://doi.org/10.1016/j.biortech.2010.08.067>
- Chi, T., Zuo, J., & Liu, F. (2017). Performance and mechanism for cadmium and lead adsorption from water and soil by corn straw biochar. *Front Environ Sci Eng* 11(2). doi:<https://doi.org/10.1007/s11783-017-0921-y>
- Covelo EF, Andrade ML, Vega FA (2004) Heavy metal adsorption by humic umbrilsols: selectivity sequences and competitive sorption kinetics. *J Colloid Interface Sci* 280(1):1–8. <https://doi.org/10.1016/j.jcis.2004.07.024>
- Ding W, Dong X, Ime IM, Gao B, Ma LQ (2014) Pyrolytic temperatures impact lead sorption mechanisms by bagasse biochars. *Chemosphere* 105:68–74. <https://doi.org/10.1016/j.chemosphere.2013.12.042>
- Ding Z, Hu X, Wan Y, Wang S, Gao B (2016) Removal of lead, copper, cadmium, zinc, and nickel from aqueous solutions by alkali-modified biochar: batch and column tests. *J Ind Eng Chem* 33:239–245. <https://doi.org/10.1016/j.jiec.2015.10.007>
- Dong X, Ma LQ, Li Y (2011) Characteristics and mechanisms of hexavalent chromium removal by biochar from sugar beet tailing. *J Hazard Mater* 190(1–3):909–915. <https://doi.org/10.1016/j.jhazmat.2011.04.008>
- Duan X, Pan M, Yu F, Yuan D (2011) Synthesis, structure and optical properties of CoAl₂O₄ spinel nanocrystals. *J Alloy Compd* 509(3):1079–1083. <https://doi.org/10.1016/j.jallcom.2010.09.199>
- Gao C, Cao Y, Lin J, Fang H, Luo Z, Lin Y, Huang Y (2020) Insights into facile synthesized pomelo biochar adsorbing thallium: potential remediation in agricultural soils. *Environ Sci Pollut Res Int*. <https://doi.org/10.1007/s11356-020-08595-6>
- Guo J, Yan C, Luo Z, Fang H, Hu S, Cao Y (2019) Synthesis of a novel ternary HA/Fe-Mn oxides-loaded biochar composite and its application in cadmium(II) and arsenic(V) adsorption. *J Environ Sci (China)* 85:168–176. <https://doi.org/10.1016/j.jes.2019.06.004>
- He J, Li Y, Wang C, Zhang K, Lin D, Kong L, Liu J (2017) Rapid adsorption of Pb, Cu and Cd from aqueous solutions by β -cyclodextrin polymers. *Appl Surf Sci* 426:29–39. <https://doi.org/10.1016/j.apsusc.2017.07.103>
- Huang Z, Lu Q, Wang J, Chen X, Mao X, He Z (2017) Inhibition of the bioavailability of heavy metals in sewage sludge biochar by adding two stabilizers. *PLoS ONE* 12(8):e0183617. <https://doi.org/10.1371/journal.pone.0183617>
- Jamari, J., Ali, M., Mindari, W., Handogo, R., & Suryani, E. (2016). Effect of Humic Acid on Soil Chemical and Physical Characteristics of Embankment. *MATEC Web of Conferences*, 58. doi:<https://doi.org/10.1051/mateconf/20165801028>
- Jiang J, Xu RK (2013) Application of crop straw derived biochars to Cu(II) contaminated Ultisol: evaluating role of alkali and organic functional groups in Cu(II) immobilization. *Bioresour Technol* 133:537–545. <https://doi.org/10.1016/j.biortech.2013.01.161>
- Jiang J, Xu RK, Jiang TY, Li Z (2012a) Immobilization of Cu(II), Pb(II) and Cd(II) by the addition of rice straw derived biochar to a simulated polluted Ultisol. *J Hazard Mater* 229–230:145–150. <https://doi.org/10.1016/j.jhazmat.2012.05.086>
- Jiang TY, Jiang J, Xu RK, Li Z (2012b) Adsorption of Pb(II) on variable charge soils amended with rice-straw derived biochar. *Chemosphere* 89(3):249–256. <https://doi.org/10.1016/j.chemosphere.2012.04.028>
- Jin, Z., Ping, L., & Wong, M. (2020). Systematic relationship between soil properties and organic carbon mineralization based on structural equation modeling analysis. *Journal of Cleaner Production*, 277. doi:<https://doi.org/10.1016/j.jclepro.2020.123338>
- Kasozi GN, Zimmerman AR, Kizza PN, Gao B (2010) Catechol and Humic acid sorption into a range of laboratory produced black carbons (Biochars). *Environ Sci Technol* 44:6189–6195. <https://doi.org/10.1021/es101442z>
- Kazantzis G (2000) Thallium in the environment and health effect. *Environ Geochem Health* 22:275–280. <https://doi.org/10.1023/a:1006791514080>
- Kim D-J, Shin H-J, Ahn B-K, Lee J-H (2016) Competitive adsorption of thallium in different soils as influenced by selected counter heavy metals. *Appl Biol Chem* 59(5):695–701. <https://doi.org/10.1007/s13765-016-0215-2>
- Kim, S. J., Koh, H. J., Ren, C. E., Kwon, O., Maleski, K., Cho, S. Y., Jung, H. T. (2018). Metallic Ti₃C₂T_x MXene Gas Sensors with Ultrahigh Signal-to-Noise Ratio. *ACS Nano* 12:986–993. <https://doi.org/10.1021/acsnano.7b07460>
- Lalhmunsiam, Lee, S. M., & Tiwari, D. (2013). Manganese oxide immobilized activated carbons in the remediation of aqueous wastes contaminated with copper(II) and lead(II). *Chem Eng J*, 225, 128–137. doi:<https://doi.org/10.1016/j.cej.2013.03.083>
- Langmuir I (1918) THE ADSORPTION OF GASES ON PLANE SURFACES OF GLASS, MICA AND PLATINUM. *J Am Chem Soc* 40(9):1361–1403. <https://doi.org/10.1021/ja02242a004>
- Li H, Chen Y, Long J, Li X, Jiang D, Zhang P, Gong J (2017) Removal of thallium from aqueous solutions using Fe-Mn binary oxides. *J Hazard Mater* 338:296–305. <https://doi.org/10.1016/j.jhazmat.2017.05.033>
- Li H, Li X, Xiao T, Chen Y, Long J, Zhang G, Li K (2018) Efficient removal of thallium(I) from wastewater using flower-like manganese dioxide coated magnetic pyrite cinder. *Chem Eng J* 353:867–877. <https://doi.org/10.1016/j.cej.2018.07.169>
- Luo Z, Kayiranga A, Uwiringiyimana E, Zhang Q, Yan C, Guo J, Xing B (2020) Thallium contamination in agricultural soils and associated potential remediation via biochar utilization. *Biochar* 2(1):33–46. <https://doi.org/10.1007/s42773-020-00042-6>
- Muhammad Z (2011) Effect of Agitation Speed on Adsorption of Imidacloprid on Activated Carbon. *Journal of Chemical Society of Pakistan* 33(3):305–313
- Munirathnam K, Dillip GR, Chaurasia S, Joo S. W, Deva Prasad Raju B, John Sushma N (2016) Investigations on surface chemical analysis using X-ray photoelectron spectroscopy and optical properties of Dy³⁺-doped LiNa₃P₂O₇ phosphor. *J Mol Structure*, 1118:117–123. doi:<https://doi.org/10.1016/j.molstruc.2016.04.004>
- Ndagijimana P, Liu X, Li Z, Yu G, Wang Y (2019) Optimized synthesis of a core-shell structure activated carbon and its adsorption performance for Bisphenol A. *Sci Total Environ* 689:457–468. <https://doi.org/10.1016/j.scitotenv.2019.06.235>
- Omachi H, Inoue T, Hatao S, Shinohara H, Criado A, Yoshikawa H, Prato M (2020) Concise, single-step synthesis of sulfur-enriched graphene: immobilization of molecular clusters and battery applications. *Angew Chem Int Ed Engl* 59(20):7836–7841. <https://doi.org/10.1002/anie.201913578>
- Peng H, Gao P, Chu G, Pan B, Peng J, Xing B (2017) Enhanced adsorption of Cu(II) and Cd(II) by phosphoric acid-modified biochars. *Environ Pollut* 229:846–853. <https://doi.org/10.1016/j.envpol.2017.07.004>
- Qiao J, Yu H, Wang X, Li F, Wang Q, Yuan Y, Liu C (2019) The applicability of biochar and zero-valent iron for the mitigation of arsenic and cadmium contamination in an alkaline paddy soil. *Biochar* 1(2):203–212. <https://doi.org/10.1007/s42773-019-00015-4>
- Rinklebe J, Shaheen SM, El-Naggar A, Wang H, Du Laing G, Alessi DS, Sik Ok Y (2020) Redox-induced mobilization of Ag, Sb, Sn, and Tl in the dissolved, colloidal and solid phase of a biochar-treated and un-treated mining soil. *Environ Int* 140:105754. <https://doi.org/10.1016/j.envint.2020.105754>
- Safari S, von Gunten K, Alam MS, Hubmann M, Blewett TA, Chi Z, Alessi DS (2019) Biochar colloids and their use in contaminants

- removal. *Biochar* 1(2):151–162. <https://doi.org/10.1007/s42773-019-00014-5>
- Sharma RK, Wooten JB, Baliga VL, Lin X, Geoffrey Chan W, Hajaligol MR (2004) Characterization of chars from pyrolysis of lignin. *Fuel* 83(11–12):1469–1482. <https://doi.org/10.1016/j.fuel.2003.11.015>
- Shen Z, Som AM, Wang F, Jin F, McMillan O, Al-Tabbaa A (2016) Long-term impact of biochar on the immobilisation of nickel (II) and zinc (II) and the revegetation of a contaminated site. *Sci Total Environ* 542(Pt A):771–776. <https://doi.org/10.1016/j.scitotenv.2015.10.057>
- Shirzadi H, Nezamzadeh-Ejehieh A (2017) An efficient modified zeolite for simultaneous removal of Pb(II) and Hg(II) from aqueous solution. *J Mol Liq* 230:221–229. <https://doi.org/10.1016/j.molliq.2017.01.029>
- Sizmur, T., Quilliam, R., Puga, A. P., Moreno-Jiménez, E., Beesley, L., & Gomez-Eyles, J. L. (2016). Application of Biochar for Soil Remediation. In: Guo M, He Z, Uchimiya SM (Editors), *Agricultural and Environmental Applications of Biochar: Advances and Barriers*. Soil Sci Soc Am Madison, WI pp. 295–324. doi:<https://doi.org/10.2136/sssaspecpub63.2014.0075>
- Sizmur T, Fresno T, Akgul G, Frost H, Moreno-Jimenez E (2017) Biochar modification to enhance sorption of inorganics from water. *Bioresour Technol* 246:34–47. <https://doi.org/10.1016/j.biortech.2017.07.082>
- Sun Y, Li H, Li G, Gao B, Yue Q, Li X (2016) Characterization and ciprofloxacin adsorption properties of activated carbons prepared from biomass wastes by H₃PO₄ activation. *Bioresour Technol* 217:239–244. <https://doi.org/10.1016/j.biortech.2016.03.047>
- Sun Z, Zhang Z, Zhu K, Wang Z, Zhao X, Lin Q, Li G (2020) Biochar altered native soil organic carbon by changing soil aggregate size distribution and native SOC in aggregates based on an 8-year field experiment. *Sci Total Environ* 708:134829. <https://doi.org/10.1016/j.scitotenv.2019.134829>
- Tang J, Wu W, Yu L, Fan X, Liu G, Yu Y (2019) Study on adsorption properties and mechanism of thallium onto titanium iron magnetic adsorbent. *Sci Total Environ* 694:133625. <https://doi.org/10.1016/j.scitotenv.2019.133625>
- Tang J, Zhang L, Zhang J, Ren L, Zhou Y, Zheng Y, Chen A (2020) Physicochemical features, metal availability and enzyme activity in heavy metal-polluted soil remediated by biochar and compost. *Sci Total Environ* 701:134751. <https://doi.org/10.1016/j.scitotenv.2019.134751>
- Tran HN, You S-J, Chao H-P (2016) Thermodynamic parameters of cadmium adsorption onto orange peel calculated from various methods: a comparison study. *J Environ Chem Eng* 4(3):2671–2682. <https://doi.org/10.1016/j.jece.2016.05.009>
- Tselesh AS (2008) Anodic behaviour of tin in citrate solutions: The IR and XPS study on the composition of the passive layer. *Thin Solid Films* 516(18):6253–6260. <https://doi.org/10.1016/j.tsf.2007.11.118>
- USEPA (2009) Toxicological review of thallium and compounds. Environmental Protection Agency, Washington
- Wick S, Baeyens B, Marques Fernandes M, Göttlicher J, Fischer M, Pfenninger N, Voegelin A (2020) Thallium sorption and speciation in soils: Role of micaceous clay minerals and manganese oxides. *Geochim Cosmochim Acta* 288:83–100. <https://doi.org/10.1016/j.gca.2020.07.037>
- Wu W, Li J, Lan T, Muller K, Niazi NK, Chen X, Wang H (2017) Unraveling sorption of lead in aqueous solutions by chemically modified biochar derived from coconut fiber: a microscopic and spectroscopic investigation. *Sci Total Environ* 576:766–774. <https://doi.org/10.1016/j.scitotenv.2016.10.163>
- Xiang L, Zeng LJ, Du PP, Wang XD, Wu XL, Sarkar B, Cai QY (2020) Effects of rice straw biochar on sorption and desorption of di-n-butyl phthalate in different soil particle-size fractions. *Sci Total Environ* 702:134878. <https://doi.org/10.1016/j.scitotenv.2019.134878>
- Xiao T, Yang F, Li S, Zheng B, Ning Z (2012) Thallium pollution in China: a geo-environmental perspective. *Sci Total Environ* 421–422:51–58. <https://doi.org/10.1016/j.scitotenv.2011.04.008>
- Xu P, Sun CX, Ye XZ, Xiao WD, Zhang Q, Wang Q (2016) The effect of biochar and crop straws on heavy metal bioavailability and plant accumulation in a Cd and Pb polluted soil. *Ecotoxicol Environ Saf* 132:94–100. <https://doi.org/10.1016/j.ecoenv.2016.05.031>
- Xu, J., Fan, H., Tao, X., Guo, L., & Liu, Z. (2020). Porous CoP/Ni₂P₂O₇ hollow nanospheres for high-performance supercapacitors. *Materials Letters*, 268. doi:<https://doi.org/10.1016/j.matlet.2020.127567>
- Ye L, Zhang J, Zhao J, Luo Z, Tu S, Yin Y (2015) Properties of biochar obtained from pyrolysis of bamboo shoot shell. *J Anal Appl Pyrol* 114:172–178. <https://doi.org/10.1016/j.jaap.2015.05.016>
- Yolcubal ML, Brusseau JF, Artiola P, Wierenga, & Wilson, L. G. (2004). Environmental physical properties and processes. In: *Environmental Monitoring and Characterization*. (pp. 207–239). <https://doi.org/10.1016/B978-012064477-3/50014-X>
- Yuan JH, Xu RK, Zhang H (2011) The forms of alkalis in the biochar produced from crop residues at different temperatures. *Bioresour Technol* 102(3):3488–3497. <https://doi.org/10.1016/j.biortech.2010.11.018>
- Zhang X, Yang L, Li Y, Li H, Wang W, Ye B (2012) Impacts of lead/zinc mining and smelting on the environment and human health in China. *Environ Monit Assess* 184(4):2261–2273. <https://doi.org/10.1007/s10661-011-2115-6>
- Zhang W-Z, Chen X-Q, Zhou J-M, Liu D-H, Wang H-Y, Du C-W (2013) Influence of humic acid on interaction of ammonium and potassium ions on clay minerals. *Pedosphere* 23(4):493–502. [https://doi.org/10.1016/s1002-0160\(13\)60042-9](https://doi.org/10.1016/s1002-0160(13)60042-9)
- Zhang H, Shao J, Zhang S, Zhang X, Chen H (2020b) Effect of phosphorus-modified biochars on immobilization of Cu (II), Cd (II), and As (V) in paddy soil. *J Hazard Mater* 390:121349. <https://doi.org/10.1016/j.jhazmat.2019.121349>
- Zhang, H., Lu, T., Wang, M., Jin, R., Song, Y., Zhou, Y., . . . Chen, W. (2020). Inhibitory role of citric acid in the adsorption of tetracycline onto biochars: Effects of solution pH and Cu²⁺. *Colloids and Surfaces A: Physicochemical and Engineering Aspects*, 595. doi:<https://doi.org/10.1016/j.colsurfa.2020.124731>
- Zhao, Y., Huang, L., & Chen, Y. (2017). Biochars derived from giant reed (*Arundo donax* L.) with different treatment: characterization and ammonium adsorption potential. *Environ Sci Pollut Res Int*, 24(33), 25889–25898. doi:<https://doi.org/10.1007/s11356-017-0110-3>
- Zhong L-B, Yin J, Liu S-G, Liu Q, Yang Y-S, Zheng Y-M (2016) Facile one-pot synthesis of urchin-like Fe–Mn binary oxide nanoparticles for effective adsorption of Cd(II) from water. *RSC Adv* 6(105):103438–103445. <https://doi.org/10.1039/c6ra21030a>
- Zhu L, Wang Y, He T, You L, Shen X (2016) Assessment of Potential Capability of Water Bamboo Leaves on the Adsorption Removal Efficiency of Cationic Dye from Aqueous Solutions. *J Polym Environ* 24(2):148–158. <https://doi.org/10.1007/s10924-016-0757-8>